Applied Clay Science 224 (2022) 106519

Contents lists available at ScienceDirect

Applied Clay Science

journal homepage: www.elsevier.com/locate/clay

Carbonate-free CoAl layered double hydroxides supercapacitors: Controlled precipitation via acid mediated decomplexation

Xin Ya Tan, Liviu Ungur *, Wee Shong Chin *

Department of Chemistry, National University of Singapore, 117543, Singapore

ARTICLE INFO

Keywords:
Layered double hydroxide
Controlled precipitation
Decomplexation
Supercapacitance
Pseudocapacitor

ABSTRACT

Layered double hydroxides (LDH) belong to a class of highly versatile compounds used in a myriad of applications such as energy storage, catalysis, heavy metal adsorption, etc. Given the high tunability of its structure, ranging from different metal cations to different types of intercalations, LDH can be readily customised to suit the intended applications. One of the inherent problem of LDH lies in their carbonate contamination. The presence of CO_3^{2-} anions in the intercalation greatly affects the versatility and tunability of LDH. Carbonate intercalation also poses as an interfering species for reactions involving carbonate as intermediates or final products. Unfortunately, existing synthesis procedures of LDH produce either carbonates during the precipitating process or poorly crystallised LDH that absorbs atmospheric carbon dioxide to form carbonates during the drying process; either way results in carbonate contaminated LDH. In this work, we address the problem with the use of ethylenediamine (EDA) complexation followed by controlled decomplexation to prepare CoAl LDH (LDH-EDA). It is shown that the obtained LDH-EDA is carbonate-free and outperforms the CoAl LDH obtained using conventional urea method (LDH-Urea) in terms of crystallinity, surface area and pseudocapacitive properties. Through a detailed experimental and computational study of the preparation mechanism, we propose that ammonium nitrate acts as an acid that mediates the decomplexation of the cobalt (II) trisethylenediamine complex, freeing Co^{2+} ion in a control manner for the second precipitation process. The multistep process has allowed a controlled rate of formation of LDH, resulting in the highly crystalline LDH-EDA microstructures with pure nitrate intercalation and a flower-like morphology.

1. Introduction

Layered double hydroxides (LDH) are layered structures made up of edge-sharing octahedrons of mixed metal hydroxides separated by interlayer of hydrated anions. It is defined by the general formula $[M^{2+}_{1-x}M^{3+}_x(OH)_2]^{x+}$ $[(A^{n-})^{x/n}, y\ H_2O]$ where M^{2+} is divalent metal ion, M^{3+} is trivalent metal ion and A^{n-} is interlayer anion (Evans and Slade, 2006). The LDH structure provides much versatility for intended applications, e.g. the pair of metal cations can be altered to optimize the electrochemical and photochemical properties. Depending on the ratio of the cations used, LDH of varying metal cation ratio can be prepared, resulting in different electrochemical characteristics of the LDH (Gupta et al., 2008). As for the anions, they can be exchanged with other anions or other guest molecules to alter the structural and chemical properties of the LDH. The order of affinity of anions to the LDH layers has been studied experimentally and computationally as follows: $CO_3^{2-} > OH^- > F^- > Cl^- > Br^- > NO_3^-$ (Miyata, 1983; Costa et al., 2012).

Due to the high affinity of carbonate anions in the layers, LDH applications that capitalize on anion exchange within the interlayer space will be impeded, e.g. removal of oxyanions (Goh et al., 2008), drug transport (Bi et al., 2014) and interlayer polymerization of polymers (Wang and Ohare, 2012). The presence of strongly-held carbonate anions not only affects the efficacy of these applications, it also limits the formation of LDH composites relying on such exchange reactions. Besides, carbonate intercalation may constitute also a possible source of carbon contamination for CO_2 capturing and reduction reactions (Chong et al., 2018). Such contamination may have resulted in false positive or overstated values, giving rise to repeatability issues in the literatures. Hence, it is clear that having carbonate intercalation in the LDH layers poses a troubling issue for research in various different fields.

To overcome the aforementioned problems, research attention has been focused on the preparation of LDH that are intercalated with other anions, e.g. nitrate, which have relatively lower affinity to the LDH layers. A common method to prepare nitrate intercalated LDH is via co-

* Corresponding authors at: Department of Chemistry, 3 Science Drive 3, Faculty of Science, National University of Singapore, 117543, Singapore.
E-mail addresses: chmlu@nus.edu.sg (L. Ungur), chmcws@nus.edu.sg (W.S. Chin).

https://doi.org/10.1016/j.clay.2022.106519
Received 22 November 2021; Received in revised form 4 April 2022; Accepted 12 April 2022
Available online 27 April 2022

precipitation, where a precipitant such as sodium hydroxide or aqueous ammonia is used (Forano et al., 2013). This method is versatile in the choices of metal cations and the intercalated anion species, since most LDHs can be precipitated out at a given pH range. A major limitation of this technique, however, is the uncontrollable growth of LDH, resulting in crystals of low crystallinity and without apparent morphology. In a study conducted by Hibino, air-dried LDH of lower crystallinity were found to have significantly lower anion exchange abilities when compared to the equivalent LDH of higher crystallinity (Hibino, 2015). It was proposed that atmospheric carbon dioxide dissolved in water forms carbonate anions that bind strongly to the LDH surface throughout the slow drying process. This shows that high crystallinity and controllable growth play important roles in maintaining the durability and effectiveness of LDH in its applications, but these are qualities that standard co-precipitation methods cannot provide.

The controlled release of ammonia, via the heating of urea, as a source of hydroxide ions has been used to provide highly crystalline plate-like LDH crystals (Liu et al., 2006). However, a shortcoming of this urea hydrolysis method is the production of carbonate anions as a by-product that intercalate in the LDH layers. Iyi et al. have attempted to replace urea with hexamethylenetriamine (HMT) (Iyi et al., 2004). Unlike urea, HMT hydrolyses to form ammonia and formaldehyde, of which the latter is not intercalated directly into the interlayer space. The final samples obtained were still carbonate-intercalated, nevertheless, as carbonate anion may be formed via the oxidation of methanoic acid due to the oxidation of formaldehyde (Moore, 2011). Although the use of an acid salt solution to de-intercalate LDH has shown to be effective, this technique is not very widely used, mainly because the acidic solution might compromise the LDH structure (Hibino, 2014).

In 2011, Inayat et al. reported the synthesis of nitrate intercalated ZnAl LDH, employing the refined urea method (Inayat et al., 2011). They observed that, in the presence of ammonium ions and excess nitrate ions, it is possible to obtain nitrate-intercalated ZnAl LDH. However, the synthesised ZnAl LDH samples consisted of thick slabs of LDHs adhered together. Such morphology does not benefit the usage of LDHs in applications where surface area or active sites play an important role. The existing synthesis methods have difficulty in synthesising carbonate-free LDHs that are crystalline with well-defined morphology.

Herein, we report a method to synthesize carbonate-free CoAl LDH using ethylenediamine (EDA) and ammonium nitrate. Our experimental and computational studies elucidated a controlled complexation-decomplexation route and the role of NH_4NO_3 in mediating the reaction. The prepared LDH was found to be nitrate intercalated and have a flower-like morphology with high surface area. When compared with LDH synthesised using the urea method, the LDH synthesised with EDA was found to be superior in terms of crystallinity, surface area and pseudocapacitive properties.

2. Experimental section

2.1. Materials used

All reagents used including $Co(NO_3)_2.6H_2O$, $Al(NO_3)_3.9H_2O$, NH_4NO_3, ethylenediamine (EDA), *Nafion* and urea were obtained from Sigma-Aldrich and used without further purification.

2.2. Preparation procedures

2.2.1. Synthesis of CoAl LDH with EDA

In a typical procedure, 6.68 mL of EDA was dissolved and stirred in 25 mL of deionised water in a two-neck round bottom flask (RBF). A certain concentration of NH_4NO_3 was dissolved in 50 mL of deionised water and then split into two portions to dissolve $Co(NO_3)_2.6H_2O$ (6.39 g) and $Al(NO_3)_3.9H_2O$ (5.45 g) separately. After all solids have dissolved completely, the $Al(NO_3)_3.9H_2O$ solution was first added to the mixture in RBF followed by the $Co(NO_3)_2.6H_2O$ solution. The reaction mixture was then topped with 25 mL of deionised water and then purged with N_2 gas. After purging, the solution was stirred at 350 rpm and refluxed at ~100–101 °C for 48 h. (Colour changes at various stages of the synthesis are illustrated in *Supporting Information Fig. S1*). After cooling to room temperature, the product was isolated, washed with deionised water and anhydrous ethanol by centrifugation at 4000 rpm for 5 min until the supernatant appeared clear. The pink CoAl LDH obtained were left to dry in vacuum overnight. In the elucidation of reaction mechanism, LDH samples prepared with varying concentration (0.05 to 2.0 M) of NH_4NO_3 were studied.

2.2.2. Synthesis of CoAl LDH with urea

The synthesis route was adapted from Inayat et al. (Inayat et al., 2011). The reaction set up is the same as that for LDH-EDA, with the exception that 6.01 g of urea was used instead of EDA. In our discussions, this sample is labelled as LDH-Urea when compared with LDH-EDA above.

2.2.3. Electrode preparation

Ni foam cut into 1.5 cm by 0.5 cm was used as the current collector for the working electrode. The Ni foam strips were first soaked in 1 M HCl for 15 min to remove any surface oxide present. This was followed by washing and sonication in water, ethanol and acetone for 5 min respectively. The washed Ni foam strips were then dried under vacuum for 24 h. About 82 mg of the active material consisting of the LDH, carbon black and Nafion in weight ratios of 80: 10: 10 was suspended in ethanol and sonicated for 5 min before being drop casted onto a 0.5 cm × 0.5 cm area of the prepared Ni foam. The ratio of ethanol added to the mixture is about 1 mL to every 0.09 g of active material.

2.3. Structural characterisation

Powder x-ray diffraction (XRD) patterns were recorded on a Bruker D2 diffractometer with Cu Kα radiation ($\lambda = 0.15406$ nm) in the 2θ range from 5° to 80° at a scan rate of 0.05° s^{-1}. The intercalated anions were studied by Fourier transform infrared (FT-IR) with Bruker Alpha FT-IR spectrometer using KBr plates within the wavenumber region of 400 cm^{-1} to 4000 cm^{-1}. Morphology of the samples were studied using JEOL JSM 6700-F scanning electron microscope (SEM). For elemental analysis, 5 mg of the sample was digested with HNO_3/HCl (1:3 *v*/v) and topped up to 10 mL of ultrapure water. The digested sample was analysed with Perkin Elmer Optima 5300DV inductively coupled plasma-optical emission spectrometer (ICP-OES). Thermogravimetric analysis (TGA) was carried out using a Discovery Thermogravimetric Analyser. Sample was heated in air from room temperature to 900 °C at a ramping rate of 10 °C/min. Surface area of the samples were measured using the Quantachrome AutoSorb IQ surface area analyser at 77 K. Surface areas of the samples were then calculated by applying the Brunauer–Emmett–Teller (Brunauer et al., 1938) (BET) adsorption function onto the isotherm. The pore size and pore volume information were obtained by using the Barrett-Joyner-Halenda (BJH) method.

2.4. Electrochemical measurements

The electrochemical properties of the LDH samples were measured using a Metrohm Autolab Potentiostat in a three-electrode configuration. The as-prepared Ni foam substrate containing the active material was used as the working electrode (WE), a 3 M Ag/AgCl electrode was used as the reference electrode (RE) and a platinum rod was used as the counter electrode (CE). Cyclic voltammetry (C*V*) was conducted in the potential window of -0.1 to 0.55 V (vs Ag/AgCl) at potential scan rates of 1, 2, 5, 10 mV/s.

To compare the electrocapacitive properties of LDH-EDA and LDH-Urea, galvanostatic charge-discharge (GCD) measurements were performed in a potential window of 0.0 V to 0.4 V at constant current densities of 0.5, 1, 2, 5 and 10 A/g. The specific capacitance of the

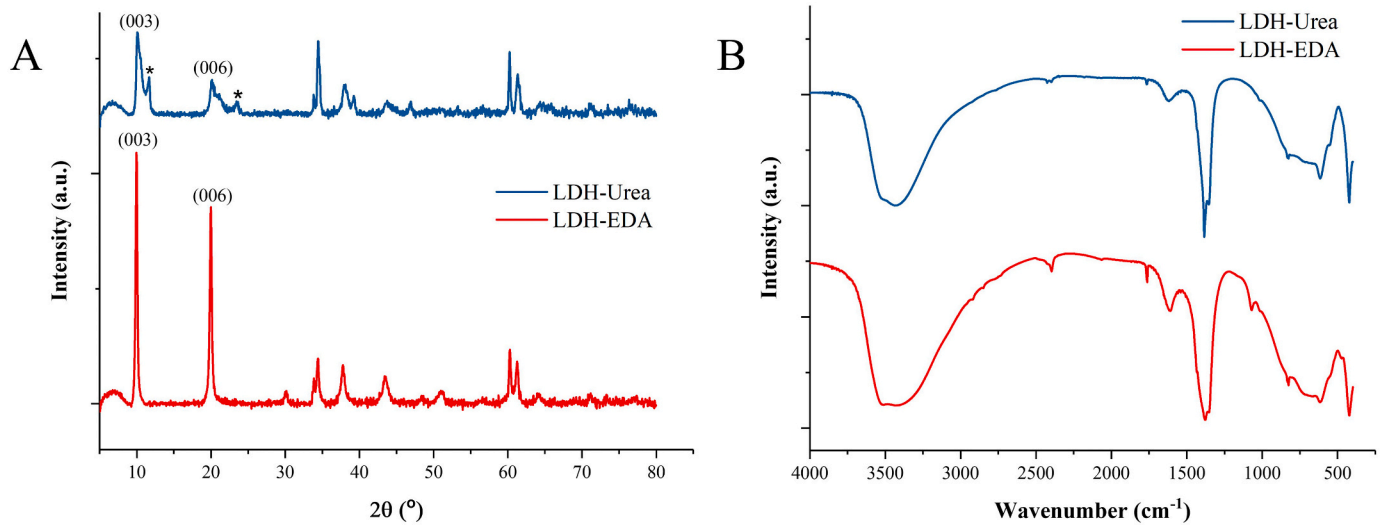

Fig. 1. A comparison of (A) XRD patterns and (B) FT-IR spectra of LDH-EDA and LDH-urea.

sample was then calculated using the following formula:

$$C_s = I\,\Delta t/m\Delta V$$

where I is the current applied, Δt is the time taken for the complete discharge, m is the mass of active material and ΔV is the potential window.

2.5. Computational details

All structures were optimised without symmetry constraints on Gaussian 16(Frisch et al., 2016) at DFT level using the B3LYP functional (Vosko et al., 1980; Lee et al., 1988; Becke, 1993; Stephens et al., 1994) with the 6-311G(d,p) basis set (Wachters, 1970; Hay, 1977; Krishnan et al., 1980; Raghavachari and Trucks, 1989). Solvent effects are considered using the default model with water as the solvent used. Tight convergence criteria were used. All transition structures and minima were fully characterized by harmonic analysis. For each located transition structure, only one imaginary frequency was obtained, and the corresponding vibration was found to be associated with nuclear motion along the reaction coordinate.

3. Results and discussion

3.1. Structural comparison between LDH-EDA and LDH-urea

3.1.1. X-ray diffraction

Fig. 1A compares XRD patterns of the LDH-EDA and LDH-Urea samples prepared. The first diffraction peak corresponds to the (003) plane, which is indicative of the basal distance between the intercalated layers and thus its 2θ value is anion-dependent. It is known that the (003) plane of a carbonate intercalated CoAl LDH appears at 2θ = 11.52° (JCPDS 51–0045). The (003) plane of LDH-EDA sample was found at a lower value of 2θ = 10.01°, suggesting that carbonate ions are not the main intercalated species in this sample. The LDH-Urea sample, on the other hand, showed a small peaks (*) at ~11.5°. This agrees with reported finding that LDH prepared from urea hydrolysis is often contaminated with carbonate anions.

The XRD peaks of LDH-EDA are also visibly sharper than those of LDH-Urea, indicating much better crystallinity of the products synthesised via the EDA route. It is likely that the mixed intercalation of LDH-Urea by nitrate and carbonate anions resulted in regions of lattice strains and ambiguous interlayer spacings, hence giving rise to broadened diffraction peaks.

3.1.2. Fourier transform infrared spectroscopy

The presence of nitrate anion was further confirmed using FT-IR as shown in Fig. 1B. Both spectra show the nitrate asymmetric vibrational

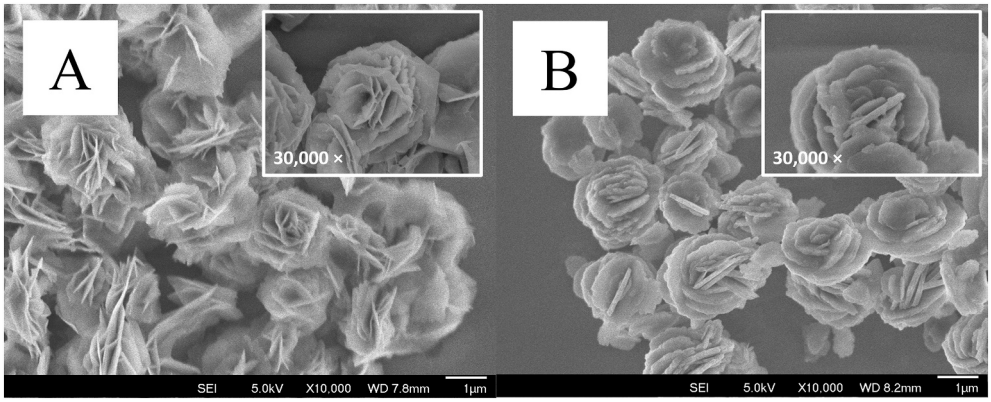

Fig. 2. SEM images of (A) LDH-EDA and (B) LDH-Urea respectively. Insets show the respective zoom-in images of the flower-like morphology and the much thinner petals in (A).

Table 1
Elemental mole ratios and mass percentage data, together with the BET analysis results of LDH-EDA and LDH-urea.

Sample	Co (ppm)	Al (ppm)	Co/Al mole ratio	Mass percentage of Co (%)	Mass percentage of Al (%)	Surface area (m^2/g)	Pore volume (cc g^{-1})	Pore radius /Å
LDH-EDA	151	42	1.61	32.2	9.16	41.1	0.349	27.0
LDH-Urea	161	52	1.42	29.8	9.62	23.9	0.095	14.9

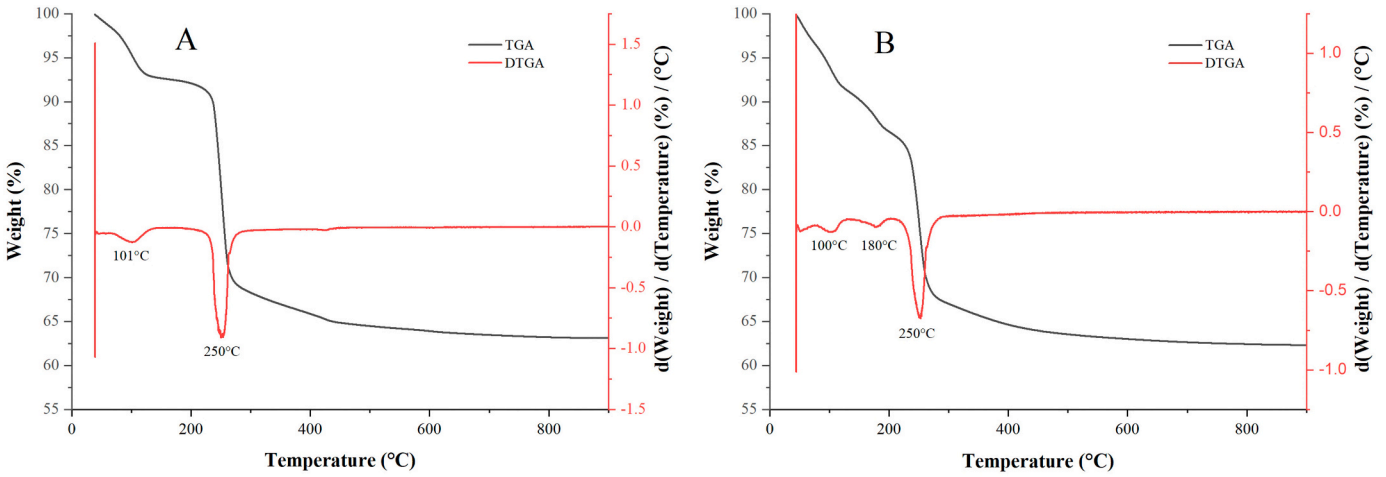

Fig. 3. TGA and DTGA curves of (A) LDH-EDA and (B) LDH-urea.

mode at ~1380 cm^{-1} as well as out-of-plane bending mode at ~830 cm^{-1} (Kloprogge et al., 2002). Additionally, we observe an OH stretching vibration at ~3470 cm^{-1} and water bending mode at 1640 cm^{-1}. This indicates the presence of water molecules within the LDH-EDA and LDH-Urea layers. While XRD data suggested low amount of carbonate intercalation in LDH-Urea sample, the stronger N—O asymmetric vibrational mode at 1380 cm^{-1} may have covered the weaker C—O vibrational mode at 1360 cm^{-1} in FT-IR.

3.1.3. Scanning electron microscopy

From the SEM images in Fig. 2, it is observed that both synthesis routes give rise to irregularly shaped plates that stack up to form flower-like structures. Such structures are known to give high surface area and possess an interconnected open porous morphology, which is known to facilitate electron transport and ion diffusion (Zhang et al., 2016). As shown clearly in the insets, the LDH-EDA sample has visibly thinner petals compared to those of LDH-Urea. A similar thinning effect on LDH crystallites was observed by Yang et al in their synthesis of NiMn LDH with EDA. They proposed that EDA adsorbs onto the surface of the growing LDH crystallites, hence preventing further growth of the plates (Yang et al., 2019). We postulate that similar surface adsorption, together with the controlled decomplexation of the cobalt complex (vide infra), will allow LDH-EDA to grow into such intricate morphology. Since LDH-EDA has much thinner morphology, we thus expect LDH-EDA to have higher surface area as compared to LDH-Urea, and this is supported by the BET surface area analysis data shown in the next section and Table 1.

3.1.4. Surface area and pore size analysis

BET analysis (Table 1, details given in *Supporting Information Fig. S2*) confirmed that LDH-EDA (41.3 m^2/g) has a much higher surface area as compared to LDH-Urea (23.0 m^2/g). This significantly higher surface area will increase the accessibility of the Co sites, and in turn improve the pseudocapacitive performance of the LDH-EDA. The isotherms obtained for both samples have clear hysteresis loops that are characteristic of Type IV adsorption isotherms, which are associated to mesoporous materials (Thommes et al., 2015). Pore distribution analysis using the BJH method also concurs with this finding (refer to *Supporting Information Fig. S3*).

3.1.5. Elemental and thermogravimetry analysis

Elemental analysis data in Table 1 showed that the stoichiometric ratio of Co:Al in both samples deviate slightly from the feed ratio of 1.5:1. As shown by the TGA and differential TGA (DTGA) curves in Fig. 3, LDH-EDA and LDH-Urea both exhibit a total mass loss of 36.9% and 37.71% respectively. As expected, a thermal event occurred at ~100 °C, corresponding to the removal of physisorbed water on the LDH surfaces. The main mass loss for both samples is owing to the removal of hydroxyl groups and interlayer anions at 250 °C (Pérez-Ramírez et al., 2001). An additional DTGA peak was observed at 180 °C for LDH-Urea, most probably associated with the removal of interlayer water molecules within the LDH (Babay et al., 2015). The relatively clean TGA plot suggests that there is no other contamination or remnant EDA in the LDH-EDA sample after washing. The residual mass can be attributed to $Co_xAl_1O_4$ where x is the Co/Al mole ratio determined by elemental analysis (Pérez-Ramírez et al., 2001; Abdel-Aziz et al., 2020). Using the residual mass percentage and Co/Al mole ratio, the percentage mass of Co for each sample could be estimated as shown in Table 1. The result suggests that, in addition to better crystallinity and higher surface area, the prepared LDH also contains slightly higher Co content via the EDA synthesis route.

3.2. The electrochemical properties of LDH-EDA and LDH-urea

As a pseudocapacitor, the capacitance of CoAl LDH material depends mainly on its surface redox reactions. It has been proposed that cobalt hydroxide undergoes the following redox reactions (Cao et al., 2004):

(1) $Co(OH)_2 + OH^- \rightleftarrows CoOOH + H_2O + e^-$
(2) $CoOOH + OH^- \rightleftarrows CoO_2 + H_2O + e^-$

The CV plots in Fig. 4A show good symmetry between the reduction and oxidation peaks, indicating good electrochemical reversibility of CoAl LDH as a pseudocapacitative material. It is noted that LDH-EDA

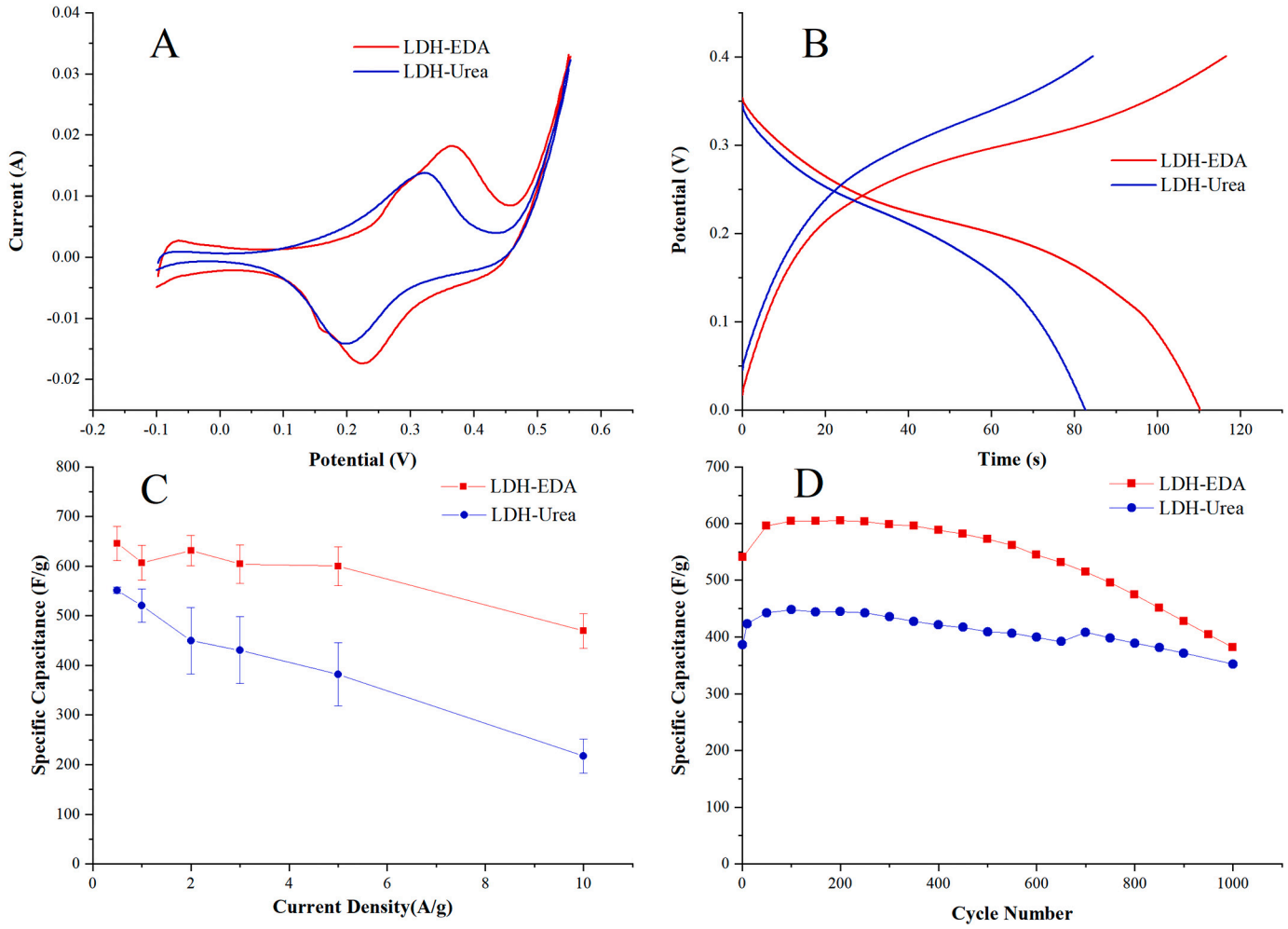

Fig. 4. Comparison of the electrochemical properties of LDH-EDA and LDH-Urea. (A) CV curves at 2 mV/s in 6 M KOH, (B) GCD curves at 2 A/g in 6 M KOH, (C) Current stability plot of each LDH sample, (D) Cycling stability curves at 5 A/g in 6 M KOH.

has visibly higher peak currents as compared to LDH-Urea. This confirms that LDH-EDA has more effective charge transfer within the sample, attributed to reasons discussed earlier. By comparing the area bounded by the CV curves, it is evident that LDH-EDA has a larger specific capacitance value as compared to LDH-Urea.

The GCD curves of LDH-EDA and LDH-Urea charged at 2A/g are shown in Fig. 4B. LDH-EDA was found to have a specific capacitance of 631 F/g while that of LDH-Urea is 449 F/g. When the samples are charged at 0.5, 1, 2, 5 and 10 A/g, the corresponding specific capacitance values are 646, 607, 631, 600 and 469 F/g for LDH-EDA respectively. The corresponding values for LDH-Urea, on the other hand, are 551, 520, 449, 382 and 217 F/g. On a per mole of Co basis (refer to Table 1), the LDH-EDA values are ~1.4 times (144F/111F) higher than the LDH-Urea values. This difference in charge storage abilities can be attributed to the difference in the surface area of the samples.

Fig. 4C shows the specific capacitance values of both samples with increasing current densities. Lower current densities often yield better

Table 2
Comparison of specific capacitance of CoAl-LDH based electrodes in the literature.

	LDH	Surface area/m^2g^{-1}	Specific capacitance/Fg^{-1}	Cycling stability	Ref.
CoAl LDH	LDH-EDA	41.1	631 ($2Ag^{-1}$)	70.7% (1000 cycles)	This work
	$Co_{2.44}Al_1$-NO_3^- LDH	–	682 ($1Ag^{-1}$)	–	(Huang et al., 2015)
	CoAl-CO_3^{2-} LDH	–	799 ($1Ag^{-1}$)	73.7% (5000 cycles)	(Wang and Jin, 2021)
	$Co_{1.77}Al_1$-CO_3^{2-} LDH	–	ca. 750 ($1Ag^{-1}$)	50.0% (2000 cycles)	(Seijas-Da Silva et al., 2020)
	CoAl-CO_3^{2-} LDH	72.7	984 ($1Ag^{-1}$)	89.1% (15,000 cycles)	(Jing et al., 2019)
	CoAl-CO_3^{2-} LDH	23.8	620 ($1Ag^{-1}$)	73.8% (1000 cycles)	(Huang et al., 2017)
	CoAl-CO_3^{2-} LDH	152	838 ($1Ag^{-1}$)	95.0% (20,000 cycles)	(Zai et al., 2017)
	CoAl- OH^- LDH	–	169 ($1Ag^{-1}$)	100% (900 cycles)	(Su and Zhang, 2007)
	CoAl-CO_3^{2-} LDH	–	335 ($0.8Ag^{-1}$)	44.9% (200 cycles)	(Hu et al., 2013)
CoAl LDH composites	Co-Al LDH/rGO-3	–	1492 ($1Ag^{-1}$)	94.3% (5000 cycles)	(Li et al., 2019)
	CoAl-LDH/PG-4	–	864 ($1Ag^{-1}$)	90.1 (10,000 cycles)	(Zhang et al., 2017)
	GSP-LDH	35.7	1043 ($1Ag^{-1}$)	88% (3000 cycles)	(Wu et al., 2015)
	CoAl LDH-NS/rGO	42.8	1296 ($1Ag^{-1}$)	90.5 (1000 cycles)	(Huang et al., 2015)
	CoAl LDH/graphene	23.4	712 ($1Ag^{-1}$)	82.1 (2000 cycles)	(Zhang et al., 2012)

specific capacitance, as more time is given for the electrolyte ions to diffuse and come into contact with the electroactive areas of the LDH (Li et al., 2014a). On the other hand, a large drop in specific capacitance is usually observed at high current density due to an increase in the degree of IR drop, which has a positive relationship with the intrinsic conductivity of the material. Since LDH-EDA retained a higher specific capacitance when current density increases, we can conclude that LDH-EDA has a higher intrinsic conductivity as compared to LDH-Urea. While LDH-EDA has a higher overall capacitance as compared to LDH-Urea, it has a slightly lower cycling stability (Fig. 4D). After 1000 charge-discharge cycles at 5 A/g, LDH-EDA achieved a stability retention of 70.7% of its specific capacitance while LDH-Urea achieved a stability retention of 91.2%.

We can attribute the variation in stability retention of the two samples to the difference in their aluminium content. Meng et al has observed that, with extended soaking of CoAl LDH in a strong basic medium, the LDH structure collapses to form β-$Co(OH)_2$ due to the leaching of Al^{3+} ions (Hu et al., 2013). β-$Co(OH)_2$ has a smaller d-spacing and does not allow any anion intercalation in between the hydroxide layers (Xu and Zeng, 1999). This will severely inhibit the electron transport and ion diffusion processes within the material, hence resulting in a degradation of the electrochemical performance of CoAl LDH. Since LDH-EDA has lesser Al content as compared to LDH-Urea, the onset of its structural collapse will occur earlier than LDH-Urea. This thus results in a lower cycling stability for LDH-EDA.

In Table 2, we summarize some recent reported electrochemical results of CoAl LDH in the literature. LDH-EDA performs reasonably well among the other CoAl LDH counterparts. At first glance, it may seem that LDH-EDA does not perform as well relative to the other nitrate-intercalated $Co_{2.44}Al_1$-NO_3^-LDH. However, when we factor in the difference in Co/Al ratio of the two samples (Co/Al for LDH-EDA = 1.61, for $Co_{2.44}Al_1$-NO_3^- LDH = 2.44), it becomes clear that more charges were stored per unit of Co in the LDH-EDA sample. This confirms that the open structure of LDH-EDA does expose more Co sites for ion exchange.

The specific capacitance of CoAl LDH falls short when compared with LDH composites. This is not surprising due to the increased conductivity and improved structural stability offered by the added carbonaceous material in the composites. Nevertheless, the synthesis of LDH composites will require an exfoliation of the LDH layers before introducing the guest material. Exfoliation is often achieved with either the use of formaldehyde or separation of the layers with surfactants (Woo et al., 2011; Li et al., 2014b; Mao et al., 2017; Chen et al., 2020). The latter approach depends on how well the initial anions can be deintercalated from the layers. In this aspect, our proposed synthesis with nitrate intercalation will also provide clear advantage.

3.3. Proposed mechanism

Unlike most metal hydroxide syntheses reported earlier, where EDA often acted as a source of nitrogen dopant (Guo et al., 2018), chelating agent (Sampanthar and Zeng, 2002) or surface adsorbate (Yang et al., 2019), EDA is acting both as a base and a chelating agent in our proposed LDH reaction. This proposition is supported by some single crystals obtained from the supernatant left behind after the isolation of LDH-EDA. The single crystal structure (see *Supporting Information Fig. S4 and Table S1*) corresponded well to cobalt tris(ethylenediamine) complex with empirical formula $Co(en)_3Na(H_2O)_6Cl_7$, where *en* is the abbreviation for the $NH_2(CH_2)_2NH_2$ group of EDA.

The above finding suggests that the supernatant contains $[Co(en)_3]^{3+}$. Given that $[Co(en)_3]^{2+}$ could have oxidised to the more stable $[Co(en)_3]^{3+}$ complex in the presence of atmospheric oxygen, this indirectly confirms that, under inert reaction conditions, Co^{2+} also reacted with EDA to form $[Co(en)_3]^{2+}$ complex:

$$Co^{2+} + 3\,en \rightleftharpoons [Co(en)_3]^{2+}$$

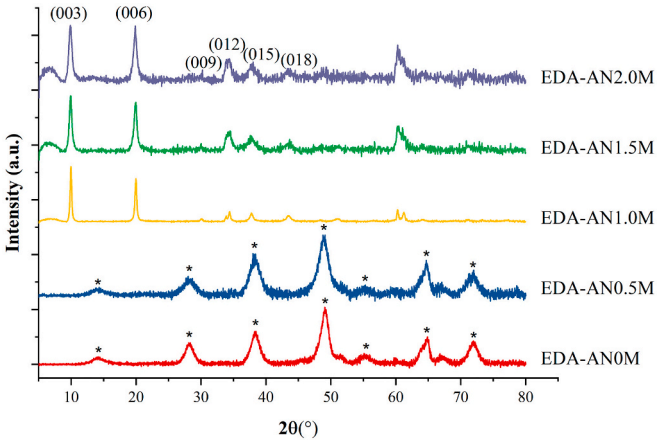

Fig. 5. XRD patterns of solid products isolated with varying concentrations of NH_4NO_3. Boehmite γ-AlOOH peaks (JCPDS card no. 49–1033) are labelled with *.

While the roles of the other reagents are known, e.g. metal salts provide the respective metal cations, the role of NH_4NO_3 in the proposed synthesis seems to be unclear. In order to determine its role, the NH_4NO_3 concentration was varied and samples labelled as EDA-AN*x*M for NH_4NO_3 concentration $x = 0$, 0.5, 1.0, 1.5 and 2.0 M, respectively, were studied.

As confirmed by the XRD patterns in Fig. 5, CoAl LDH (JCPDS card no: 51–0045) was produced only when the concentration of NH_4NO_3 was 1.0 M and above. At lower NH_4NO_3 concentration, only Boehmite (γ-AlOOH, JCPDS card no. 49–1033) was formed. As seen in Table 3, the final pH of all reaction mixtures was within the range of pH 5–10 for γ-AlOOH precipitation, but LDH formation is observed only when pH is below 6.85.

In summary, experimental results confirmed that CoAl LDH is formed only at high NH_4NO_3 concentration. Single crystal study, on the other hand, indicated the formation of $[Co(en)_3]^{2+}$ complex in the reaction solution. While EDA is expected to play a role in surface adsorption that controls the growth of crystal during precipitation, we postulate that the detachment of the *en* ligands under acidic condition further regulates the release of Co^{2+} ions for the LDH formation. Such kinetic control of a multistep reaction is key to nanostructure fabrication. The significance is well demonstrated by the epoxide route method proposed to control the size of the LDH single crystals formed (Oestreicher and Jobbágy, 2013, 2019; Oestreicher et al., 2014). In our proposed route, kinetic control further facilitates the growth into favourable crystal morphology.

A computational study was designed to elucidate the decomplexation of a single amine arm of the *en* ligand from the $[Co(en)_3]^{2+}$ complex; geometry optimization was performed in the presence and the absence of protonation (see *Supporting Information Fig. S5–6 and Table S2–3*). From the DFT calculated energy profile diagram shown in Fig. 6, it is clear that the activation energy of the protonated route is comparatively lower than that of the non-protonated route. Furthermore, the product formed from the protonated route is significantly more stable than that of the non-protonated route. Hence, overall, the DFT results indicated that the protonation route is more favourable than the non-protonated route. Theoretical study thus supports the proposed decomplexation process mediated by the acidic environment and concurs with the observations in Fig. 5 and Table 3.

At higher pH conditions, it is likely that the lack of free Co^{2+} ions prohibited the formation of CoAl LDH, hence only γ-AlOOH was obtained. The protonation of *en* ligands is expected to occur more readily as the concentration of NH_4NO_3 increases. This will in turn increases the rate of decomplexation of Co^{2+} and the precipitation process. Since particle size is often affected by the reaction kinetics, we noted that the

Table 3
Initial and final pH of reaction mixture using different concentration of NH_4NO_3.

Sample label	Initial pH of reaction mixture	Final pH of reaction mixture	CoAl LDH produced	FWHM of CoAl LDH (003) peak in XRD
EDA-AN0M	8.59	8.53	No	–
EDA-AN0.5M	8.51	7.55	No	–
EDA-AN1.0M	8.44	6.85	Yes	0.30
EDA-AN1.5M	8.40	6.59	Yes	0.50
EDA-AN2.0M	8.38	6.53	Yes	0.56

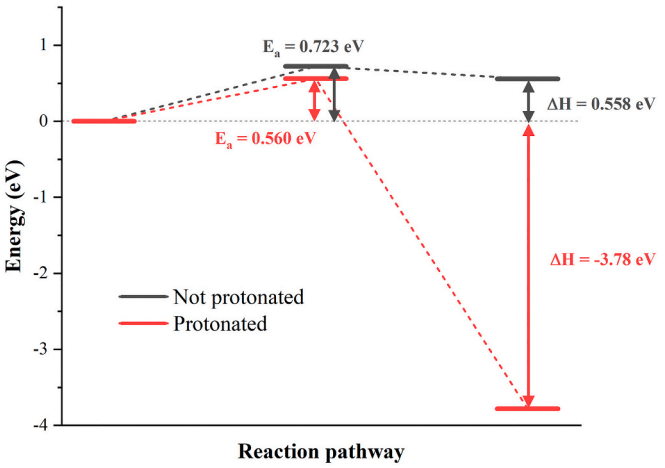

Fig. 6. DFT calculated energy profile of the decomplexation of the amine arm of the en ligand from the $[Co(en)_3]^{2+}$ complex, with and without protonation.

FWHM of the (003) XRD peaks becomes broader with increasing concentration of NH_4NO_3 (Table 3). This is in line with our postulation, as broadened XRD peaks are indicative of smaller particle sizes. The morphology of the crystals, however, may be compromised at fast reaction rates. SEM images in Fig. 7 showed that, whereas EDA-AN1.0M sample formed flower-like nanostructures, EDA-AN1.5M and EDA-AN2.0M gave particles agglomerated in clumps without a clear morphology.

Considering the above observations and the LDH formation mechanism (Boclair and Braterman, 1999) proposed by Boclair et al, we postulate a reaction scheme as illustrated in Fig. 8. Firstly, complexation of Co^{2+} to $[Co(en)_3]^{2+}$ occurs together with the formation of $Al(OH)_3$ crystals. In the presence of NH_4^+ ions, the chelating en ligand is protonated and decomplexation occurs. Since each cobalt ion is chelated by three en ligands, we anticipate the complexation and decomplexation processes to be kinetically controlled. The free Co^{2+} ions will then add onto the $Al(OH)_3$ precipitates to form CoAl LDH. The excess EDA molecules can adsorb onto the surface of the LDH sheets, thus limiting crystal growth in the z direction (Yang et al., 2019). This, together with the slow decomplexation kinetics, results in LDH sheets with thin morphology and intricate morphology.

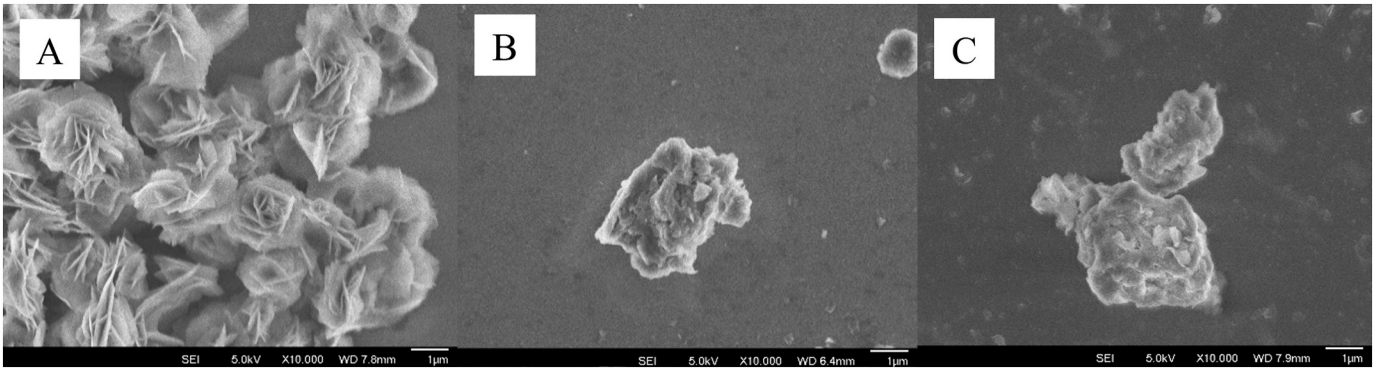

Fig. 7. SEM images of EDA-AN prepared with NH_4NO_3 of (A) 1.0 M, (B) 1.5 M and (C) 2.0 M.

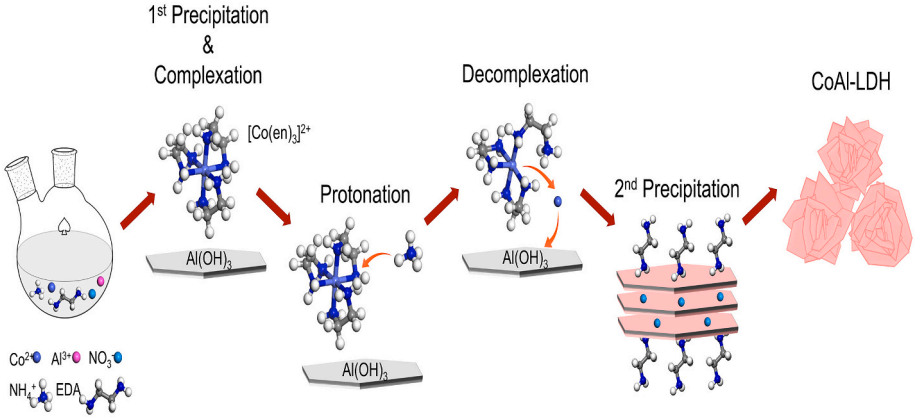

Fig. 8. Schematic for the formation of CoAl LDH flower-like morphology via complexation-decomplexation of Co^{2+} with EDA.

4. Conclusions

In summary, a new and simple approach using EDA as both the base and chelating agent is reported to synthesize nitrate-intercalated CoAl LDH microstructures. In comparison to the CoAl LDH prepared using urea, the EDA synthesised LDH was free of carbonate intercalation and had a higher surface area. We have also shown that the LDH-EDA prepared this way outperformed LDH-Urea in electrochemical properties, largely due to its increased surface area and exposed Co sites. The decomplexation of $[Co(en)_3]^{2+}$ mediated by the addition of NH_4NO_3 as a source of protons helps to slow down the growth of the crystal plates. Together with the adsorption of EDA onto the surface, the growth of the LDH crystallites is controlled and flower-like microstructures with thin petals were obtained.

We believe that further study of the controlled precipitation via complexation-decomplexation mechanism can help to produce more refined carbonate-free microstructures for LDH of various metal ion pairings. Given the various fields LDH can be applied in, such carbonate-free synthesis technique would be invaluable in ensuring the versatility of the synthesised LDH materials.

CRediT authorship contribution statement

Xin Ya Tan: Conceptualization, Investigation, Writing – original draft. **Liviu Ungur:** Methodology, Supervision, Writing – review & editing. **Wee Shong Chin:** Methodology, Supervision, Writing – review & editing.

Declaration of Competing Interest

There are no conflicts to declare.

Acknowledgements

This research work was supported by the Singapore Ministry of Education Academic Research Fund Tier 1 grants: R-143-000-634-112, R-143-000-A65-133 and R-143-000-A80-114. Ab initio calculations were performed on the ASPIRE-1 cluster (www.nscc.sg) under the project 11001278.

Appendix A. Supplementary data

Supplementary data to this article can be found online at https://doi.org/10.1016/j.clay.2022.106519.

References

Abdel-Aziz, M.H., Zoromba, M.S., Bassyouni, M., Zwawi, M., Alshehri, A.A., Al-Hossainy, A.F., 2020. Synthesis and characterization of Co-Al mixed oxide nanoparticles via thermal decomposition route of layered double hydroxide. J. Mol. Struct. 1206, 127679 https://doi.org/10.1016/j.molstruc.2020.127679.

Babay, S., Bulou, A., Mercier, A.M., Toumi, M., 2015. The decomposition of the layered double hydroxides of Co and Al: phase segregation of a new single phase spinel oxide. Spectrochim. Acta Part A Mol. Biomol. Spectrosc. 141, 80–87. https://doi.org/10.1016/j.saa.2015.01.021.

Becke, A.D., 1993. Density-functional thermochemistry. III. The role of exact exchange. J. Chem. Phys. 98, 5648–5652. https://doi.org/10.1063/1.464913.

Bi, X., Zhang, H., Dou, L., 2014. Layered double hydroxide-based nanocarriers for drug delivery. Pharmaceutics 6, 298–332. https://doi.org/10.3390/pharmaceutics6020298.

Boclair, J.W., Braterman, P.S., 1999. Layered double hydroxide stability. 1. Relative stabilities of layered double hydroxides and their simple counterparts. Chem. Mater. 11, 298–302. https://doi.org/10.1021/cm980523u.

Brunauer, S., Emmett, P.H., Teller, E., 1938. Adsorption of gases in Multimolecular Layers. J. Am. Chem. Soc. 60, 309–319. https://doi.org/10.1021/ja01269a023.

Cao, L., Xu, F., Liang, Y.Y., Li, H.L., 2004. Preparation of the novel nanocomposite Co (OH)2/ultra-stable Y zeolite and its application as a supercapacitor with high energy density. Adv. Mater. 16, 1853–1857. https://doi.org/10.1002/adma.200400183.

Chen, C., Tao, L., Du, S., Chen, W., Wang, Y., Zou, Y., Wang, S., 2020. Advanced exfoliation strategies for layered double hydroxides and applications in energy conversion and storage. Adv. Funct. Mater. 30, 1–18. https://doi.org/10.1002/adfm.201909832.

Chong, R., Su, C., Du, Y., Fan, Y., Ling, Z., Chang, Z., Li, D., 2018. Insights into the role of MgAl layered double oxides interlayer in Pt/TiO2 toward photocatalytic CO2 reduction. J. Catal. 363, 92–101. https://doi.org/10.1016/j.jcat.2018.04.020.

Costa, D.G., Rocha, A.B., Souza, W.F., Chiaro, S.S.X., Leitão, A.A., 2012. Comparative Structural, thermodynamic and electronic analyses of Zn-Al-A n- hydrotalcite-like compounds (A n-Cl -, F -, Br -, OH -, CO 32- or NO 3-): an ab initio study. Appl. Clay Sci. 56, 16–22. https://doi.org/10.1016/j.clay.2011.11.014.

Evans, D.G., Slade, R.C.T., 2006. Structural aspects of layered double hydroxides. In: Duan, X., Evans, D.G. (Eds.), Layered Double Hydroxides. Springer, Berlin Heidelberg, Berlin, Heidelberg, pp. 1–87. https://doi.org/10.1007/430_005.

Forano, C., Costantino, U., Prévot, V., Gueho, C.T., 2013. Layered double hydroxides (LDH). Dev. Clay Sci. https://doi.org/10.1016/B978-0-08-098258-8.00025-0.

Frisch, M.J., Trucks, G.W., Schlegel, H.B., Scuseria, G.E., Robb, M.A., Cheeseman, J.R., Scalmani, G., Barone, V., Petersson, G.A., Nakatsuji, H., Li, X., Caricato, M., Marenich, A.V., Bloino, J., Janesko, B.G., Gomperts, R., Mennucci, B., Hratchian, H. P., Ortiz, J.V., Izmaylov, A.F., Sonnenberg, J.L., Williams-Young, D., Ding, F., Lipparini, F., Egidi, F., Goings, J., Peng, B., Petrone, A., Henderson, T., Ranasinghe, D., Zakrzewski, V.G., Gao, J., Rega, N., Zheng, G., Liang, W., Hada, M., Ehara, M., Toyota, K., Fukuda, R., Hasegawa, J., Ishida, M., Nakajima, T., Honda, Y., Kitao, O., Nakai, H., Vreven, T., Throssell, K., Montgomery, J.A., Peralta, J.E., Ogliaro, F., Bearpark, M.J., Heyd, J.J., Brothers, E.N., Kudin, K.N., Staroverov, V.N., Keith, T.A., Kobayashi, R., Normand, J., Raghavachari, K., Rendell, A.P., Burant, J. C., Iyengar, S.S., Tomasi, J., Cossi, M., Millam, J.M., Klene, M., Adamo, C., Cammi, R., Ochterski, J.W., Martin, R.L., Morokuma, K., Farkas, O., Foresman, J.B., Fox, D.J., 2016. Gaussian 16. Gaussian, Inc, Wallingford CT.

Goh, K.H., Lim, T.T., Dong, Z., 2008. Application of layered double hydroxides for removal of oxyanions: a review. Water Res. 42, 1343–1368. https://doi.org/10.1016/j.watres.2007.10.043.

Guo, D., Xin, R., Zhang, Z., Jiang, W., Hu, G., Fan, M., 2018. Electrochimica acta N-doped hierarchically micro- and mesoporous carbons with superior performance in supercapacitors. Electrochim. Acta 291, 103–113. https://doi.org/10.1016/j.electacta.2018.08.109.

Gupta, V., Gupta, S., Miura, N., 2008. Al-substituted α-cobalt hydroxide synthesized by potentiostatic deposition method as an electrode material for redox-supercapacitors. J. Power Sources 177, 685–689. https://doi.org/10.1016/j.jpowsour.2007.10.091.

Hay, P.J., 1977. Gaussian basis sets for molecular calculations. The representation of 3d orbitals in transition-metal atoms. J. Chem. Phys. 66, 4377–4384. https://doi.org/10.1063/1.433731.

Hibino, T., 2014. Acid treatment of layered double hydroxides containing carbonate. Eur. J. Inorg. Chem. 2014, 5311–5321. https://doi.org/10.1002/ejic.201402372.

Hibino, T., 2015. Layered double hydroxide-agarose composites for water treatment: Carbonate contamination during the drying process. Appl. Clay Sci. 116–117, 93–101. https://doi.org/10.1016/j.clay.2015.08.020.

Hu, M., Ji, X., Lei, L., Lu, X., 2013. Structural and electrochemical stability of Co-Al layered double hydroxide in alkali solutions. Electrochim. Acta 105, 261–274. https://doi.org/10.1016/j.electacta.2013.04.165.

Huang, Z., Wang, S., Wang, J., Yu, Y., Wen, J., Li, R., 2015. Exfoliation-restacking synthesis of coal-layered double hydroxide nanosheets/reduced graphene oxide composite for high performance supercapacitors. Electrochim. Acta 152, 117–125. https://doi.org/10.1016/j.electacta.2014.11.085.

Huang, Q., Liu, K., He, F., Zhang, S., Xie, Q., Chen, C., 2017. Fabrication of cobalt aluminum-layered double hydroxide nanosheets/carbon spheres composite as novel electrode material for supercapacitors. Trans. Nonferrous Metals Soc. China 27, 1804–1814. https://doi.org/10.1016/S1003-6326(17)60203-6.

Inayat, A., Klumpp, M., Schwieger, W., 2011. The urea method for the direct synthesis of ZnAl layered double hydroxides with nitrate as the interlayer anion. Appl. Clay Sci. 51, 452–459. https://doi.org/10.1016/j.clay.2011.01.008.

Iyi, N., Matsumoto, T., Kaneko, Y., Kitamura, K., 2004. A novel synthetic route to layered double hydroxides using hexamethylenetetramine. Chem. Lett. 33, 1122–1123. https://doi.org/10.1246/cl.2004.1122.

Jing, C., Liu, X., Yao, H., Yan, P., Zhao, G., Bai, X., Dong, B., Dong, F., Li, S., Zhang, Y.Y., Behl, W.K., Toni, J.E., Zhang, Y.Y., Guo, H., Yuan, P., Pang, K., Cao, B., Wu, X., Shamraiz, U., Badshah, A., Raza, B., Lu, X., Xue, H., Gong, H., Bai, M., Tang, D., Ma, R., Abdollahifar, M., Zamani, R., Joy, M., Iyengar, S.J., Chakraborty, J., Ghosh, S., Lindan, P.J.D., Harrison, N.M., Xiao, R., Material, E.S., This, M.C.A., Society, T.R., Chem, J.M., Wang, J., Cui, W., Liu, Q., Xing, Z., Asiri, A.M., Sun, X., Folquer, M.E., Vilche, J.R., Arvia, A.J., Pulv, S., Leu, S., Vi, P., Jussieu, P., Studies, E., Wang, Y., Yang, W., Chen, C., Evans, D.G., Pankratov, D.A., Veligzhanin, A.A., Zubavichus, Y.V., Coronado, E., Martí-gastaldo, C., Navarro-moratalla, E., Ribera, A., Giovannelli, F., Zaghrioui, M., Autret-lambert, C., Delorme, F., Seron, A., Chartier, T., Pignon, B., Almansa, J.J., Coronado, E., Martí-gastaldo, C., Ribera, A., Gala, R., Martı, C., Ribera, A., Castro, M., Conductivity, I., Properties, M., Intissar, M., Segni, R., Payen, C., Leroux, F., Babkin, R.Y., Čižmár, E., Feher, A., Lopes, A.B., Ferreira, M.G.S., Ci, E., Ahmed, A.A., Ahmed, A.A., Salak, A.N., Vieira, D.E.L., Lukienko, I.M., Shapovalov, Y.O., Fedorchenko, A.V., Fertman, E.L., Pashkevich, Y.G., Babkin, R.Y., Shilin, A.D., Rubanik, V.V., Ferreira, M.G.S., Vieira, J.M., Boccalon, E., Gorrasi, G., Nocchetti, M., Oestreicher, V., Hunt, D., Dolle, C., Borovik, P., Carrasco, J.A., Abella, G., 2019. Phase and morphology evolution of CoAl LDH nanosheets towards advanced supercapacitor applications. CrystEngComm 21, 4934–4942. https://doi.org/10.1039/c9ce00905a.

Kloprogge, J.T., Wharton, D., Hickey, L., Frost, R.L., 2002. Infrared and Raman study of interlayer anions CO23-, NO-3, SO24-and ClO-4in Mg/Al-hydrotalcite. Am. Mineral. 87, 623–629. https://doi.org/10.2138/am-2002-5-604.

Krishnan, R., Binkley, J.S., Seeger, R., Pople, J.A., 1980. Self-consistent molecular orbital methods. XX. A basis set for correlated wave functions. J. Chem. Phys. 72, 650–654. https://doi.org/10.1063/1.438955.

Lee, C., Yang, W., Parr, R.G., 1988. Development of the Colle-Salvetti correlation-energy formula into a functional of the electron density. Phys. Rev. B 37, 785–789. https://doi.org/10.1103/PhysRevB.37.785.

Li, M., Cheng, J.P., Fang, J.H., Yang, Y., Liu, F., Zhang, X.B., 2014a. NiAl-layered double hydroxide/reduced graphene oxide composite: microwave-assisted synthesis and supercapacitive properties. Electrochim. Acta 134, 309–318. https://doi.org/10.1016/j.electacta.2014.04.141.

Li, Y., Du, N., Hou, W., Liu, S., 2014b. Synthesis and release behavior of a hybrid of camptothecin intercalated dodecyl sulfate modified layered double hydroxide. Chem. Res. Chin. Univ. 30, 137–143. https://doi.org/10.1007/s40242-014-3284-y.

Li, J., Zhang, P., Zhao, X., Chen, L., Shen, J., Li, M., Ji, B., Song, L., Wu, Y., Liu, D., 2019. Structure-controlled Co-Al layered double hydroxides/reduced graphene oxide nanomaterials based on solid-phase exfoliation technique for supercapacitors. J. Colloid Interface Sci. 549, 236–245. https://doi.org/10.1016/j.jcis.2019.04.062.

Liu, Z., Ma, R., Osada, M., Iyi, N., Ebina, Y., Takada, K., Sasaki, T., 2006. Synthesis, anion exchange, and delamination of Co-Al layered double hydroxide: Assembly of the exfoliated nanosheet/polyanion composite films and magneto-optical studies. J. Am. Chem. Soc. 128, 4872–4880. https://doi.org/10.1021/ja0584471.

Mao, N., Zhou, C.H., Tong, D.S., Yu, W.H., Cynthia Lin, C.X., 2017. Exfoliation of layered double hydroxide solids into functional nanosheets. Appl. Clay Sci. 144, 60–78. https://doi.org/10.1016/j.clay.2017.04.021.

Miyata, S., 1983. Anion-exchange properties of hydrotalcite-like compounds. Clay Clay Miner. 31, 305–311. https://doi.org/10.1346/CCMN.1983.0310409.

Moore, M.L., 2011. The Leuckart reaction. In: Organic Reactions. John Wiley & Sons, Inc, Hoboken, NJ, USA, pp. 301–330. https://doi.org/10.1002/0471264180.or005.07.

Oestreicher, V., Jobbágy, M., 2013. One pot synthesis of Mg 2 Al(OH) 6 Cl·1.5H 2 O layered double hydroxides: the epoxide route. Langmuir 29, 12104–12109. https://doi.org/10.1021/la402260m.

Oestreicher, V., Jobbágy, M., 2019. On demand one-pot mild preparation of layered double hydroxides and their hybrid forms: advances through the epoxide route. Chem. Eur. J. 25, 12611–12619. https://doi.org/10.1002/chem.201902627.

Oestreicher, V., Fábregas, I., Jobbágy, M., 2014. One-pot epoxide-driven synthesis of M 2 Al(OH) 6 Cl·1.5H 2 O layered double hydroxides: precipitation mechanism and relative stabilities. J. Phys. Chem. C 118, 30274–30281. https://doi.org/10.1021/jp510341q.

Pérez-Ramírez, J., Mul, G., Kapteijn, F., Moulijn, J.A., 2001. In situ investigation of the thermal decomposition of Co-Al hydrotalcite in different atmospheres. J. Mater. Chem. 11, 821–830. https://doi.org/10.1039/b009320n.

Raghavachari, K., Trucks, G.W., 1989. Highly correlated systems. Excitation energies of first row transition metals Sc-Cu. J. Chem. Phys. 91, 1062–1065. https://doi.org/10.1063/1.457230.

Sampanthar, J.T., Zeng, H.C., 2002. Arresting butterfly-like intermediate nanocrystals of β-Co(OH)2 via ethylenediamine-mediated synthesis. J. Am. Chem. Soc. 124, 6668–6675. https://doi.org/10.1021/ja012595j.

Seijas-Da Silva, A., Sanchis-Gual, R., Carrasco, J.A., Oestreicher, V., Abellán, G., Coronado, E., 2020. Boosting the supercapacitive behavior of CoAl layered double hydroxides via tuning the metal composition and interlayer space. Batter. Supercaps. 3, 499–509. https://doi.org/10.1002/batt.201900223.

Stephens, P.J., Devlin, F.J., Chabalowski, C.F., Frisch, M.J., 1994. Ab Initio calculation of vibrational absorption and circular dichroism spectra using density functional force fields. J. Phys. Chem. 98, 11623–11627. https://doi.org/10.1021/j100096a001.

Su, L.H., Zhang, X.G., 2007. Effect of carbon entrapped in Co-Al double oxides on structural restacking and electrochemical performances. J. Power Sources 172, 999–1006. https://doi.org/10.1016/j.jpowsour.2007.04.091.

Thommes, M., Kaneko, K., Neimark, A.V., Olivier, J.P., Rodriguez-Reinoso, F., Rouquerol, J., Sing, K.S.W., 2015. Physisorption of gases, with special reference to the evaluation of surface area and pore size distribution (IUPAC Technical Report). Pure Appl. Chem. 87, 1051–1069. https://doi.org/10.1515/pac-2014-1117.

Vosko, S.H., Wilk, L., Nusair, M., 1980. Accurate spin-dependent electron liquid correlation energies for local spin density calculations: a critical analysis. Can. J. Phys. 58, 1200–1211. https://doi.org/10.1139/p80-159.

Wachters, A.J.H., 1970. Gaussian basis set for molecular wavefunctions containing third-row atoms. J. Chem. Phys. 52, 1033–1036. https://doi.org/10.1063/1.1673095.

Wang, G., Jin, Z., 2021. Oxygen-vacancy-rich cobalt–aluminium hydrotalcite structures served as high-performance supercapacitor cathode. J. Mater. Chem. C 9, 620–632. https://doi.org/10.1039/D0TC03640D.

Wang, Q., Ohare, D., 2012. Recent advances in the synthesis and application of layered double hydroxide (LDH) nanosheets. Chem. Rev. 112, 4124–4155. https://doi.org/10.1021/cr200434v.

Woo, M.A., Song, M.S., Kim, T.W., Kim, I.Y., Ju, J.Y., Lee, Y.S., Kim, S.J., Choy, J.H., Hwang, S.J., 2011. Mixed valence Zn-Co-layered double hydroxides and their exfoliated nanosheets with electrode functionality. J. Mater. Chem. 21, 4286–4292. https://doi.org/10.1039/c0jm03430d.

Wu, X., Jiang, L., Long, C., Wei, T., Fan, Z., 2015. Dual support system ensuring porous Co-Al hydroxide nanosheets with ultrahigh rate performance and high energy density for supercapacitors. Adv. Funct. Mater. 25, 1648–1655. https://doi.org/10.1002/adfm.201404142.

Xu, Z.P., Zeng, H.C., 1999. Interconversion of Brucite-like and hydrotalcite-like phases in cobalt hydroxide compounds. Chem. Mater. 11, 67–74. https://doi.org/10.1021/cm980420b.

Yang, Z., Wang, X., Zhang, H., Yan, S., Zhang, C., Liu, S., 2019. One-step synthesis of ultrathin NiMn layered double hydroxide nanosheets for supercapacitors. ChemElectroChem 6, 4456–4463. https://doi.org/10.1002/celc.201900995.

Zai, J., Liu, Y., Li, X., Ma, Z., Feng, Qi, R., Qian, X., 2017. 3D hierarchical Co-Al layered double hydroxides with long- term stabilities and high rate performances in supercapacitors. Nano-Micro Lett. 9 https://doi.org/10.1007/s40820-016-0121-5.

Zhang, L., Zhang, X., Shen, L., Gao, B., Hao, L., Lu, X., Zhang, F., Ding, B., Yuan, C., 2012. Enhanced high-current capacitive behavior of graphene/CoAl-layered double hydroxide composites as electrode material for supercapacitors. J. Power Sources 199, 395–401. https://doi.org/10.1016/j.jpowsour.2011.10.056.

Zhang, L., Hui, K.N., Hui, K.S., Chen, X., Chen, R., Lee, H., 2016. Role of graphene on hierarchical flower-like NiAl layered double hydroxide-nickel foam-graphene as binder-free electrode for high-rate hybrid supercapacitor. Int. J. Hydrog. Energy 41, 9443–9453. https://doi.org/10.1016/j.ijhydene.2016.04.050.

Zhang, Y., Du, D., Li, X., Sun, H., Li, L., Bai, P., Xing, W., Xue, Q., Yan, Z., 2017. Electrostatic self-assembly of sandwich-like CoAl-LDH/polypyrrole/graphene nanocomposites with enhanced capacitive performance. ACS Appl. Mater. Interfaces 9, 31699–31709. https://doi.org/10.1021/acsami.7b04792.